Olivier Roussel[1,], Kai Schneider[2,3], and Henning Bockhorn[1]*

Numerical investigations on premixed spherical flames for Lewis numbers larger than unity

We present numerical simulations of premixed spherical flames under μg conditions using the thermo-diffusive approximation. The employed numerical method is based on a finite volume discretization with explicit Runge-Kutta time integration, both of second order. A multiresolution technique is used to represent the solution on an adaptive, locally refined grid, which allows efficient and accurate computations at a reduced computational cost. We study the ignition limit, i.e. the critical radius for which the flame extinguishes, for varying Lewis numbers larger than unity. We also present fully three-dimensional simulations of initially stretched spherical flames and show their relaxation towards spherical flames, which justifies the one-dimensional spherically symmetric simulations.

Authors:

1. Institut für Technische Chemie und Polymerchemie(TCP)
   Universität Karlsruhe (TH)
   Kaiserstr. 12, 76128 Karlsruhe, Germany.

2. Laboratoire de Modélisation et Simulation Numérique
   en Mécanique et Génie des Procédés, CNRS et Université d' Aix-Marseille
   38 rue Frederic Joliot-Curie, 13451 Marseille cedex 20, France.

3. Centre de Mathématiques et d'Informatique
   Université d'Aix-Marseille I,
   39 rue Frederic Joliot-Curie, 13453 Marseille cedex 13, France.

* Corresponding Adress: roussel@ict.uni-karlsruhe.de)

Paper submitted. 16.02.04
Submission of Final Revised Version: 16.02.04
Paper finally accepted: 09.02.05

1. Introduction

The study of premixed spherical flames in micro-gravity is of great interest, since only chemical reaction and heat and mass transport interact in such configurations. The micro-gravity condition is an absolute necessity, otherwise buoyant convection would destroy the symmetry of these structures. Important experimental work has been done in drop towers, in aircrafts and in the space shuttle (Ronney [10]). Numerical simulations have also been performed (Bockhorn *et al* [1], Gerlinger *et al* [4]). Both experimental and numerical investigations show the existence of stable, i.e. non-growing, spherical flame structures, the so-called "flame balls", supposing that radiative heat Posses are taken into account. In both studies, the mass diffusivity of the mixture is larger than the heat diffusivity, i.e. the Lewis number is smaller than unity. Following the theory of thermo-diffusive instabilities (Sivashinsky [13], Joulin and Clavin [8]), such mixtures belong to the family of cellular instabilities.

On the other side, for mixtures whose Lewis number is greater than unity, the stability analysis shows that spinning and pulsating flames may appear [8]. The limit between stable and pulsating planar flames has been determined using adaptive numerical simulations (Roussel and Schneider [11]). It has been shown that this limit agrees well with the asymptotic theory of Joulin-Clavin [8] for large values of the activation energy. However, to the best of our knowledge, pulsating spherical flames in micro-gravity have been neither experimentally observed, nor numerically simulated.

To perform numerical simulations of spherical flames, since very small scales are required, but only in the thin flame front region, an adaptive discretization in space is used to reduce the memory and CPU time requirements. Here, the multiresolution approach has been chosen to construct a self-adaptive strategy. The main idea is to represent a solution given on a regular fine grid as a set of data on a hierarchy of nested grids. A *discrete multiresolution analysis* is used to compress efficiently the data. This numerical approach can be seen in the spirit of Harten's pioneering work [6] for 1D hyperbolic equations, which aims at reducing the required CPU time, while keeping constant the

memory requirements. More recently, a fully adaptive version has been developed for 1D and 2D hyperbolic problems (Gottschlich-Müller and Müller [5], Cohen *et al* [3]) and extended to 3D parabolic problems (Roussel *et al* [12]). The key idea there is to represent the data on a *graded tree* structure which evolves with time, in order to reduce also memory requirements.

The aim of the present paper is to investigate the ignition limit of premixed spherical flames for Lewis numbers larger than unity. First, imposing spherical symmetry, we study the behavior of pulsating spherical flames and determine the ignition limit for varying Lewis numbers. In this study, the ignition is modelled by a spherical hot pocket containing burnt gases. Then, for spherical flames initially stretched, we study their three-dimensional behavior and determine whether the multi-dimensional perturbations are damped, as predicted by the asymptotic theory [13, 8].

The paper is organized as follows: in section 2, we present the physical problem of the pulsating spherical flames and the corresponding governing equations. In section 3, the numerical method is described, including the description of the graded tree data structure, the multiresolution analysis, the time and space discretization, and an overview of the algorithm. In section 3, numerical results for spherical flame computations in one and three dimensions are presented. Finally, we conclude and present some perspectives for future work.

2. Physical setup and governing equations

In Figure 1, a spherical flame is represented schematically together with the physical mechanisms involved. The chemical reaction occurs in the circular *flame front* delimiting the ball. Inside this ball, the gas is burnt. The rest of the domain is filled by fresh premixed gas. Close to the flame front, in the so-called *pre-heat zone*, the fresh gas is heated by thermal conduction, but no chemical reaction occurs [1].

In the present paper, we restrict ourselves to the combustion of a premixed gas which contains only two reactants and one product, the first reactant and the product being highly diluted in the second reactant. We consider that the fresh premixed gas has a Lewis number *Le* greater than unity, i.e. the thermal conduction is larger than the reactant diffusion. We also assume a slow flame propagation and the density and transport coefficients to be constant. The finite rate chemical reaction obeys a one-step Arrhenius kinetics. Radiative heat losses and gravity effects are neglected. The governing set of non-dimensional thermo-diffusive equations are [1]

$$\begin{aligned} \partial_t T - \nabla^2 T &= \omega \\ \partial_t Y - \frac{1}{Le}\nabla^2 Y &= -\omega \end{aligned} \tag{1}$$

with

$$\omega = \frac{Ze^2}{2Le} Y \exp \frac{Ze(T-1)}{1+\alpha(T-1)} \tag{2}$$

where T denotes the dimensionless temperature, Y the partial mass of the limiting reactant, ω the reaction rate, Ze the dimensionless activation energy (Zeldovich number), and α the burnt-unburnt temperature ratio. We consider that the chemical reaction occurs in a closed adiabatic cubic box Ω. Therefore we impose Neuman conditions on T and Y on the whole boundary. The initial condition chosen here corresponds to the asymptotic profile of a planar flame for $Ze \to \infty$, i.e.

$$T(t=0,r) = \begin{cases} 1 & \text{if} \quad r < R_0, \\ \exp\left(1 - \dfrac{r}{R_o}\right) & \text{if} \quad r \geq R_0, \end{cases} \tag{3}$$

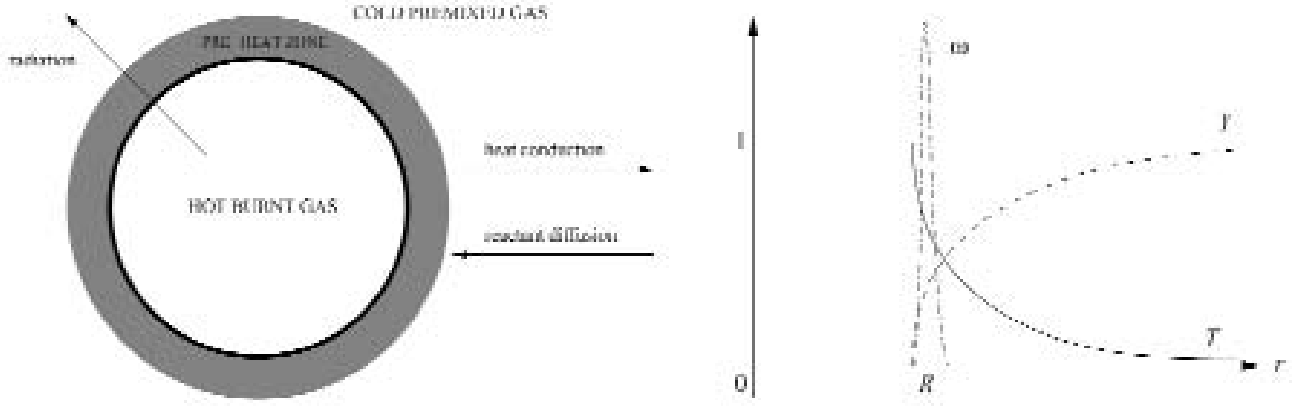

Figure 1: Left: Schematic view of a spherical flame and the involved mechanisms. Right: Sketch of the radial profiles of temperature T, partial mass of the limiting reactant Y, and reaction rate ω. Here R denotes the radius of the spherical flame.

$$Y(t=0,r)=\begin{cases}0 & \text{if} \quad r<R_0,\\ 1-\exp\left[Le\left(1-\dfrac{r}{R_o}\right)\right] & \text{if} \quad r\geq R_0,\end{cases} \tag{4}$$

where

$$r=\sqrt{x^2+y^2+z^2}$$

and R_0 denotes the initial radius of the spherical flame. For planar flames, according to Joulin and Clavin [8] an instability mechanism appears for

$$Ze\ (Le - 1) > 16, \tag{5}$$

leading to possible pulsations of flames. Pulsating planar flames have been observed experimentally in ammonia-oxygen flames standing on a cooled porous plug burner [2].

The mechanism of pulsation can be explained this way [9]: in a mixture whose Lewis number is larger that unity, the rate of heat conduction from the burnt gases into the pre-heat zone exceeds the rate of diffusion at which the reactants are transported out of it, leading to an excess enthalpy in the pre-heat zone. As a consequence, the enthalpy is decreased in the reaction zone. This implies a decrease in temperature and, due to its strong sensitivity to the temperature, the flame velocity is decreased. On the other side, the increase of enthalpy and temperature in the pre-heat zone involves an accelerated ignition of the reactant at the interphase between pre-heat and reaction zones. This is a velocity increasing effect, which counteracts the velocity decreasing in the reaction zone. Therefore, the flame velocity reaches a minimum and increases again. Depending on *Le* and *Ze* ranges, the pulsations of the flame velocity can be damped, periodic, or aperiodic [11].

3 Numerical method

The reaction-diffusion equations (1) are a system of three-dimensional non-linear parabolic PDEs and can be written in the form

$$\partial_t u - M\,\nabla^2 u = S(u) \tag{6}$$

with initial condition $u(t = 0, x) = u_o(x)$, where $u \in \mathbb{R}^2$, M is a 2×2 diagonal matrix, $x \in \Omega$, $\Omega \subset \mathbb{R}^3$, $t > 0$, and $S(u)$ is a non-linear function of u. For ease of notation, we denote by $\mathcal{D}(u) = M\nabla^2 u + S(u)$. We then have

$$\partial_t u = \mathcal{D}(u) \tag{7}$$

3.1 Adaptive multiresolution representation

The principle of the multiresolution analysis is to represent the data on a set of nested dyadic grids. The data given on a fine grid is decomposed into values on a coarser grid plus a series of differences at different levels of dyadic grids. These differences contain the information of the solution when going from a coarse to a finer grid. In particular, these coefficients are small in regions where the solution is smooth [6].

The tree structure is composed of a *root* cell, which is the basis of the tree, the *nodes* which are elements of the tree, and the *leaves* which are the upper elements. In three dimensions, a *parent* cell at a level l has always $2^3 = 8$ *children cell*s at the level $l + 1$. On the left of Figure 2, a tree structure is represented by its visible part, i.e. its leaves. For the incoming and outgoing flux computations, it may happen that a leaf at the level l has no neighbor at the same level and needs to get information from a leaf at the level $l - 1$. Therefore, *virtual* leaves are created. They only exist for the flux computation and no time evolution is made on them (Figure 2, right). In order to be *graded*, the tree must verify that each leaf at a level l has always adjacent cells of level at least equal to $l - 1$ in each direction, the diagonal being included.

Each node of the tree contains the cell-average value of u. To compute the average value of a cell at level l from the ones of cells at level $l + 1$, we use the **projection** (or restriction) operator $P_{l+1\to l}$. It is *exact* and *unique*, given that the cell-average value of a *parent* cell is the weighted average value of its *children* cell-averages. Denoting by $\bar{U}_l$ the vector of the cell-average values at the level l, we have

$$P_{l+1\to l} : \bar{U}_{l+1} \to \bar{U}_l$$

The **prediction** (or prolongation) operator $P_{l\to l+1}$ maps $\bar{U}_l$ to an approximation $\hat{U}_{l+1}$ of $\bar{U}_l$. In contrast with the projection operator, there is an infinite number of choices for the definition of $P_{l\to l+1}$. Nevertheless, in order to be applicable in a graded tree structure, it needs to be local, i.e. based on an interpolation using the s nearest neighbours in each direction, and *consistent with the projection,* i.e. $P_{l+1\to 1}$ o $P_{l\to l+1} = Id$.

The *detail* is the difference between the exact and predicted values. The vector $\bar{D}_l$ of the details at level l therefore verifies

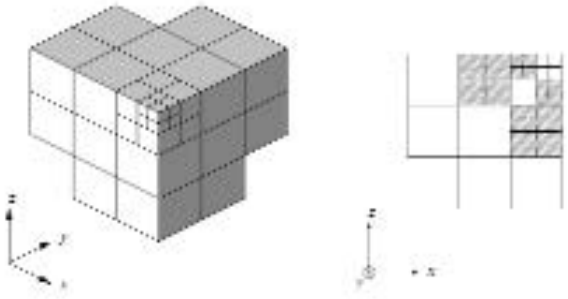

Figure 2: Left: graded tree structure in 3D. Right: leaves (plain) and virtual leaves (striped) the (x, z) plan.

$\bar{D}_l = \bar{U}_l - \dot{U}_l$. Thanks to the consistency assumption, the sum of the details on all the children of a parent cell is equal to zero [6]. Therefore, in three dimensions, the knowledge of the 8 *children* cell-averages of a given *parent* cell is equivalent to the knowledge of the parent cell-average and 7 *details*, i.e. $\bar{U}_l \leftrightarrow (\bar{U}_{l-1}, \bar{D}_l)$. Repeating the operation on L levels, one gets the so-called *multiresolution transform* [6]

$$\mathrm{M} : \bar{U}_L \rightarrow (\bar{U}_0, \bar{D}_1, \ldots \bar{D}_L) \tag{8}$$

The **threshold** operator $\mathbf{T}(\varepsilon)$ consists in removing leaves where details are smaller than a prescribed tolerance ε, without violating the graded tree data structure. After thresholding, one more level is also added to forecast the tree evolution at the next time step. The choice for an accurate tolerance is described in [12].

3.2 Time and space discretization - Algorithm

At each time step $t^n = n\Delta t$, a time evolution is performed on the leaves of the tree. Integrating (7) on a leaf $\Omega_{l,i,j,k}$, and dividing it by the cell volume $|\Omega_{l,i,j,k}| = \int_{\Omega,\, l,i,j,k} dx\, dy\, dz$ yields

$$\partial_t \bar{u}_{l,i,j,k}(t) = \bar{\mathcal{D}}_{l,i,j,k}(t) \tag{9}$$

where $\bar{u}_{l,i,j,k}$ (resp. $\bar{\mathcal{D}}_{l,i,j,k}$ denotes the cell-average value of u (resp. $\mathcal{D}$ (u)) on the cell $\Omega_{l,i,j,k}$.

Time integration is performed with a second-order explicit Runge-Kutta scheme. For space discretization, we use a second-order accurate centered scheme in each direction for the viscous term. For the computation of the source term, we approximate the cell-average value of u with the value of u at the center of the cell, which also yields a second-order accuracy.

In the following, we briefly summarize the algorithm. For more details we refer the reader to [12]. First, depending on the initial condition, an *initial graded tree* is created. Then, given the graded tree structure, a *time evolution* is made on the *leaves*. Finally, details are computed by *multiresolution transform*, in order to *remesh* the tree.

Denoting by $\bar{\mathbf{E}}(\Delta t)$ the discrete *time evolution* operator, the global algorithm can schematically be summarized by

$$\bar{u}^{n+1} = \bar{\mathbf{M}}^{-1} \cdot \mathbf{T}(\varepsilon) \cdot \bar{\mathbf{E}}(\Delta t) \cdot u^n \tag{10}$$

where $\bar{\mathbf{M}}$ is the multiresolution transform operator, and $\mathbf{T}(\varepsilon)$ is the *threshold operator* with tolerance ε.

4. Numerical results

In this part, we consider a reactive gaseous mixture whose Zeldovich number and burnt-unburnt temperature ratio are respectively $Ze = 10$ and $\alpha = 0.8$.

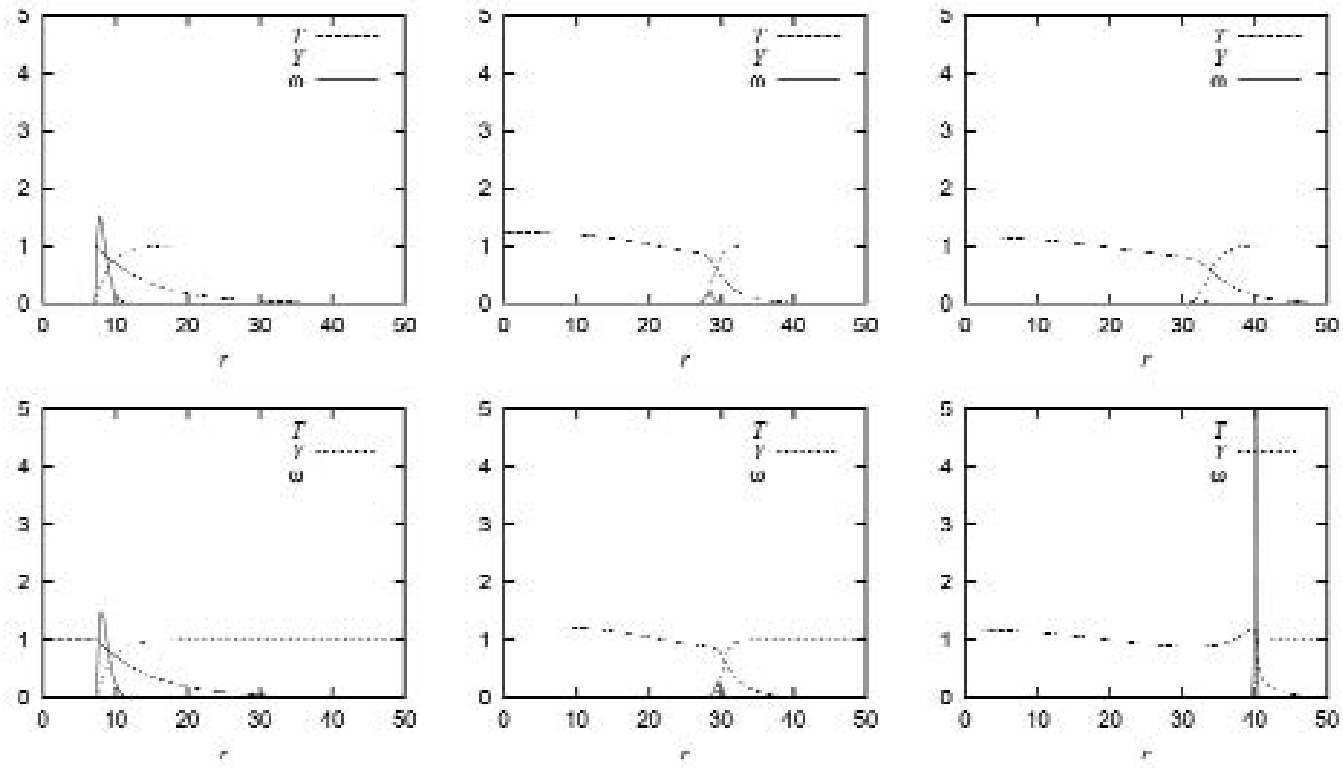

Figure 3: Radial profiles of temperature T, partial mass of the limiting fresh reactant Y, and reaction rate ω for $R_0 < R_c$ (top) and $R_0 > R_c$ (bottom) at t = 0 (left), t = 24 (center), and t = 52 (right), Le = 4, Ze = 10.

4.1 Ignition of spherically symmetric flames

We consider that the initial hot pocket of burnt gas is spherical and impose spherical symmetry. Hence the problem becomes one-dimensional. The computational domain is set to Ω = [0,140]. The chosen fresh mixture has a Lewis number that verifies (5). For a general description of the ignition problem using a hot pocket of burnt gases, we refer the reader to He-Clavin [7].

According to the asymptotic theory [8] and the numerical simulations [11], pulsating instabilities may appear for such mixtures. However, since the thermal conduction is larger than the reactant diffusion, the initial hot spot may extinguish in the velocity decreasing phase before the first pulsation appears. Therefore, we also need to determine the critical ignition radius R_c of the hot spot.

In Figure 3, the profiles of T, Y, and ω are given at different times for Le = 4. In Figure 3 (bottom), the initial radius R_0 is larger than R_c and a pulsation appears, whereas in Figure 3 (top), it is smaller than R_c and the flame extinguishes. In this configuration, the computed critical ignition radius is R_c = 7.4. Between t = 0 and t = 24, in both cases, the flame velocity is first strongly increased, due to the accelerated ignition in the pre-heat zone, and then strongly decreased, due to the strong thermal conduction from the flame front region to the pre-heat zone (see also Figure 4, center). As already remarked for planar flames [11], during the first velocity increasing phase, the temperature in the reaction zone exceeds the one in the burnt gas region. Consequently, the burnt gas receives heat from the flame front region by thermal conduction and the temperature there exceeds 1 (Figure 3, center). The main difference in the spherical case is that this thermal energy accumulates in the center of the spherical flame. This explains why the temperature in the burnt gas region remains larger than 1, even when the flame is extinguished (Figure 3, right).

The instant t = 24 approximately corresponds to the *critical point* in the flame propagation: if the reaction rate is below a certain limit, the chemical reaction may not restart. This is the case in the top picture of Figure 3, and we observe that the reaction rate is decreased until the extinction. On the other side, in the bottom picture, the reaction rate slightly exceeds the critical value, and due to the phenomenon of *accelerated ignition* previously described, the reaction rate is strongly increased (Figure 3, bottom right). In Figure 4, the average radius of the spherical flame R_f and the corresponding flame velocity V_f are plotted. Here R_f is defined using a barycentric formula, the weight being the reaction rate, i.e.

$$R_f = \frac{\sum_{i\varepsilon\mathcal{L}(\Omega)} \overline{\omega}_i r_i}{\sum_{i\varepsilon\mathcal{L}(\Omega)} \overline{\omega}_i}, \tag{11}$$

where $\mathcal{L}(\Omega)$ denotes the ensemble of *leaves* of the computational domain Ω, r_i the distance between the center of the leaf i and the center of the spherical flame, and $\overline{\omega}_i$ the average reaction rate in the leaf i. Let us remark that the reaction rate is always positive. The choice for this quantity enables us to determine the average radius even when the flame is no more spherical. It will be used in the next part for spherical flames initially stretched. The flame velocity is defined as the time derivative

$$V_f = \frac{\partial R_f}{\partial t} \tag{12}$$

of the average radius, i.e.

For $R_0 > R_c$, we observe, as in the planar case [11], periodic pulsations of the spherical flame (Figure 4, center). We remark that the average radius never decays. The flame velocity has a pulsating behavior, but it is always positive. In the case where the flame extinguishes, we remark that the average radius very slowly decays. This means that the reaction rate tends towards zero but the flame front approximately remains at the same position.

Finally, we determine the critical ignition radius R_c for varying Lewis numbers (Figure 4, right side), and remark that R_c

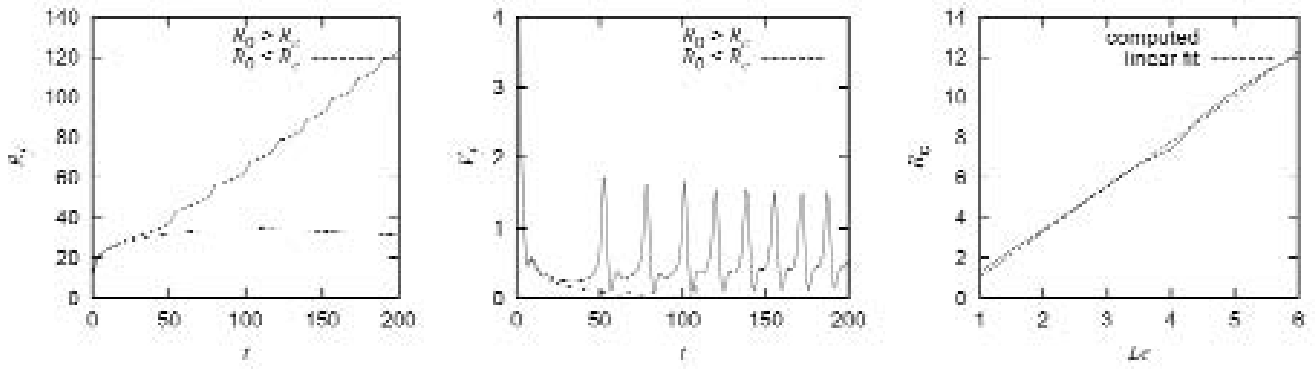

Figure 4: Left: Time evolution of the flame-ball radius R_f for an initially spherical flame, Le = 4, Ze = 10. Center: Time evolution of the flame velocity V_f for an initially spherical flame, Le = 4, Ze = 10. Right: Critical ignition radius R_c in function of the Lewis number for Ze = 10.

approximately grows linearly with Le in the range $1 \leq Le \leq 6$ for $Ze = 10$.

4.2 Ignition of perturbated spherical flames

We consider the same fresh mixture as in the previous case, i.e. $Le = 4$ and $Ze = 10$, but this time the initial spherical hot pocket is stretched to an ellipsoid, and a rotation is applied so that the axes of the ellipsoid are not lined up with the directions of the mesh. The computational domain is $\Omega = [-50, 50]^3$. The isosurfaces of temperature and the reaction rate in the plan $y = 0$ are plotted in Figure 5. The finest resolution would correspond to $(2^8)^3 = 256^3$ cells. On average we only use 5.9% cells. Comparing the elapsed CPU time with the one obtained by the same finite volume scheme on the finest grid, we get a CPU compression of 18.4%. We observe that the initial perturbation is damped and that the ellipsoidal flame relaxes to a spherical one. This result is predicted by the asymptotic theory [13, 8], which states that multi-dimensional perturbations are amplified only when $Ze\ (Le - 1) < -2$. Here we have $Ze\ (Le - 1) = 30$. In the same time, we observe a pulsation, characterized by a decreasing and increasing reaction rate (Figure 5, bottom). The average radius R_f and the flame velocity V_f are plotted in Figure 6. These quantities are computed the same way as in the previous subsection. As initial condition, we choose an ellipsoidal hot spot whose volume τ_0 is smaller (dotted lines) or larger (plain lines) than $\tau_c = (4/3)\pi R_c^3$, where R_c denotes the critical ignition radius computed for initially spherical flames. We observe that the same value of the critical ignition radius determines the ignition limit of spherical flames initially stretched. A difference in this case is that, for the extinguishing flame, the average radius tends towards zero and, consequently, the flame velocity, defined in (12), becomes negative. For longer times, the flame becomes spherical, and the problem becomes spherically symmetric.

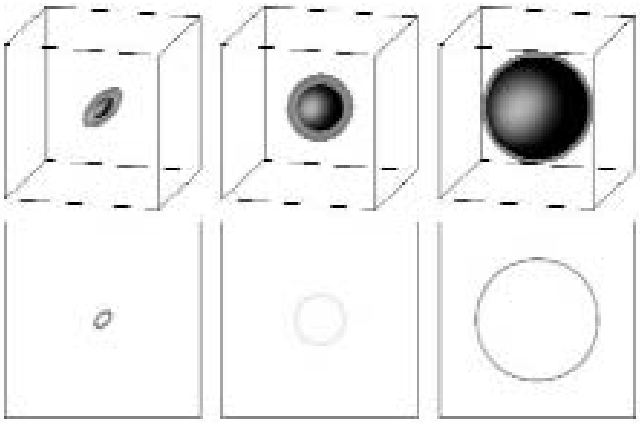

Figure 5: Pulsation of a spherical flame initially stretched. Top: Isosurfaces of temperature T = 0.5 (black) and T = 0.1 (gray) at t = 0 (left), t = 30 (center), and t = 60 (right). Bottom: Slice y = 0: Corresponding reaction rate ω from 0 (white) to 1 (black), Le = 4, Ze = 10, $\Omega = [-50, 50]^3$.

5. Conclusion

By means of numerical simulation, we have studied the unsteady behaviour of premixed spherical flames in microgravity for slowly diffusing reactants, i.e. for mixtures whose Lewis number is larger than unity. A prominent example are lean mixtures of heavy hydrocarbons. The thermo-diffusive equations have been solved numerically using an adaptive multiresolution scheme with automatic local grid simulations, in one-dimension imposing spherical symmetry and computations, have been carried out.

For spherically symmetric flames, we have established the ignition limit for $Ze = 10$ and $1 \leq Le \leq 6$. We have found that the critical ignition radius, defined as the initial burnt gas, grows linearly with the Lewis number. Using fully three-dimensional simulations, we have shown that an ellipsoidal flame relaxes

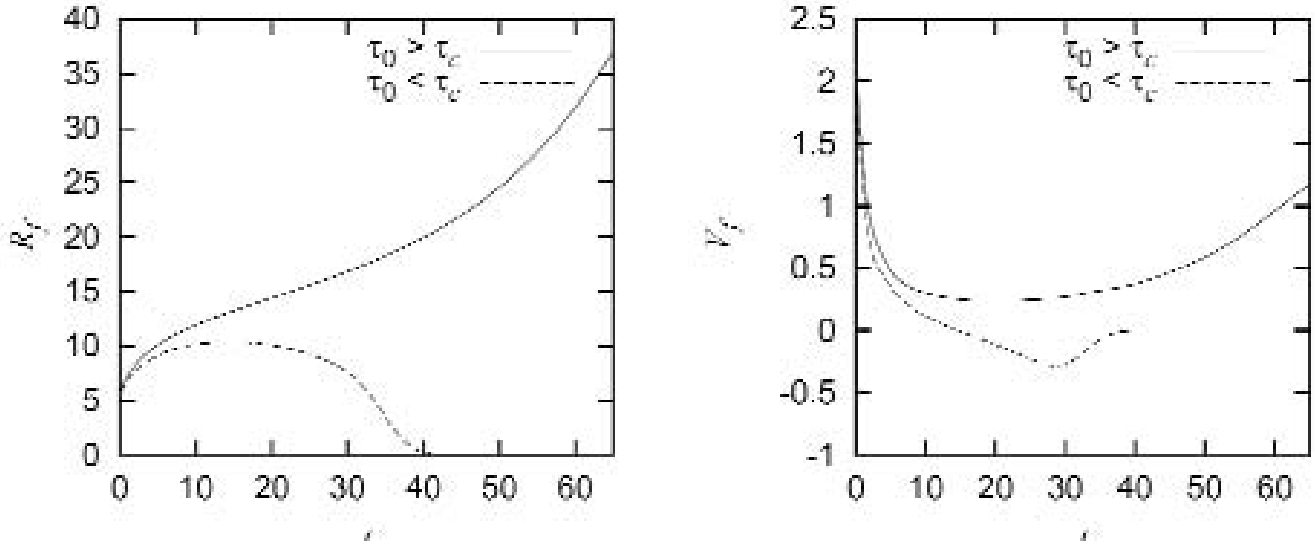

Figure 6: Left: Time evolution of the average radius R_f for a spherical flame initially stretched. Right: Time evolution of the flame velocity V_f, Le = 4, Ze = 10, $\Omega = [-50, 50]^3$.

towards a spherical one. This justifies the one-dimensional simulations imposing spherical symmetry.

The above results have been performed for adiabatic flames, i.e. radiative heat losses have been neglected, and the dimensionless activation energy was set to 10. This motivates future work that will focus on studying the influence of radiation, considering various ranges of Zeldovich numbers. Finally, we will also consider the influence of g-jitter effects, as encountered in drop towers, parabolic flights and in the international space station (IIS).

Acknowledgements

We thankfully acknowledge financial support from the French-German CNRS-DFG Programme "LES of complex flows" and from ESA/ESTEC Topical Team "Numerical and experimental studies of instabilities in lean gas-phase combustion".

References

[1] *H. Bockhorn, J. Fröhlich, and K. Schneider.* An adaptive two-dimensional wavelet-vaguelette algorithm for the computation of flame balls. Combust. Theory Modelling, 3:1-22, 1999.

[2] *P. Clavin.* Dynamic behaviour of premixed flame fronts in laminar and turbulent flows. Prog. Energy Combust. Sci., 11:1-59, 1985.

[3] *A. Cohen, S. M. Kaber, S. Müller, and M. Postel.* Fully adaptive multiresolution finite volume schemes for conservation laws. Math. Comp., 72:183-225, 2002.

[4] *W. Gerlinger, K. Schneider, J. Fröhlich, and H.Bockhorn.* Numerical simulations on the stability of spherical flame structures. Combust. Flame, 132:247-271, 2003.

[5] *B. Gottschlich-Müller and S. Müller.* Adaptive finite volume schemes for conservation laws based on local multiresolution techniques. In M. Fey and R. Jeltsch, editors, Hyperbolic problems: Theory, numerics, applications, pages 385-394. Birkhäuser, 1999.

[6] *A. Harten.* Multiresolution algorithms for the numerical solution of hyperbolic conservation laws. Comm. Pure Appl. Math., 48:1305-1342, 1995.

[7] *L. He and P. Clavin.* Premixed Hydrogen-Oxygen flames. part II: Quasi-isobaric ignition near the flammability limit. Combust. Flame, 93:408 420, 1993.

[8] *G. Joulin and P. Clavin.* Linear stability analysis of nonadiabatic flames: diffusional-thermal model. Combust. Flame, 35:139 153, 1979.

[9] *B. Rogg.* The effect of Lewis number greater than unity on an unsteady propagating flame with one-step chemistry. In N. Peters and J. Warnatz, editors, Numerical methods in laminar flame propagation, volume 6 of Notes on numerical fluid mechanics, pages 38 48. Vieweg, 1982. [10]

[10] *P. D. Ronney*. Near-limit flame structures at low Lewis number. Combust. Flame, 82:1-14, 1990.

[11] *O. Roussel and K. Schneider:* Adaptive numerical simulation of pulsating planar flames for large Lewis and Zeldovich ranges. submitted to Comm. Nonlinear Sci. Numer. Simul., 11:463-480,2006

[12] *O. Roussel, K. Schneider, A. Tsigulin, and H. Bockhorn.* A conservative fully adaptive multiresolution algorithm for parabolic PDEs. J. Comput. Phys., 188(2):493-523, 2003.

[13] *G. I. Sivashinsky.* Diffusional-thermal theory of cellular flames.Combust. Sci. Tech., 15:137-146, 1977.